ORIGINAL PAPER

Impact of Co–Ni substitution on the structural and dielectric properties of calcium copper titanate

S Sharma[1], T T T Carol[1], J Mohhamed[2], D Basandrai[1] and A K Srivastava[1]*

[1]Department of Physics, Lovely Professional University, Phagwara, Punjab 144411, India

[2]Department of Physics, Faculty of Science, Federal University Dutse, P.M.B., 7156, Dutse, Jigawa State, Nigeria

Abstract: CCTO ceramics are known for their high dielectric constant and low loss, making them potential candidates for use in various electronic and energy storage applications. The dielectric properties of CCTO ceramics can be tuned by doping of various elements. In addition to the dielectric properties, Co–Ni substitution has also been found to affect other properties of CCTO ceramics, such as the thermal and electrical conductivity. Therefore, Co–Ni substitution can be a useful strategy for tailoring the properties of CCTO ceramics for specific applications. In this research work, the sol–gel auto-combustion technique is used for the synthesis of Co–Ni-substituted calcium copper titanate, $Ca_{(1-x)}Co_{(x)}Cu_3Ti_{(4-y)}Ni_{(y)}O_{22}$ ($x = 0.0/y = 0.0$, $x = 0.1/y = 0.3$ and $x = 0.2/y = 0.4$). X-ray diffraction, Fourier transform infrared spectroscopy, field emission scanning electron microscopy, and impedance analyzer have all been used to examine the structural and dielectric properties of synthesized samples. X-ray diffraction study shows the presence of crystalline structure of calcium copper titanate. The presence of peaks at 422 cm^{-1}, 503 cm^{-1}, and 506 cm^{-1} in FTIR spectra also confirms the presence of CCTO. The Debye-type relaxation technique and Maxwell–Wagner model describe dielectric characteristics. The grain boundary resistance (R_{gb}) significantly contributes to the dielectric properties of synthesized calcium copper titanate as seen by the Cole–Cole plot.

Keywords: High frequency; Sol–gel auto-combustion; Structural and dielectric properties

1. Introduction

Nowadays, attention is increasing toward electronic devices with performance technologies. Expanding of technological innovation requires materials with giant permittivity and less tan δ worth scaling down the size of electronic parts. The material, for example, barium titanate, has a perovskite structure and is known to have captivating dielectric characteristics but shows a strong dependence on temperature and frequency. Contrarily, calcium copper titanate (CCTO) is unaffected by temperature (100-600 K) and frequency (10^2–10^6 Hz) and has a large dielectric constant (102–106 MHz), making it an attractive material for use in electronic devices. It can potentially increase the performance and efficiency of electronic devices such as capacitors and sensors. CCTO exhibits ferroelectric behavior. The unique properties of CCTO make it a

promising candidate for use in various applications, from electronic devices to energy storage and sensing technologies. Moreover, its enormous dielectric loss restrains its utilization for electronic device fabrication, high-capacity memory devices, gas sensors, and microwave devices [1].

Despite various endeavors, the origin of its massive permittivity stays a secret. Recently, the concept of grain boundaries between semiconducting grains and the internal barrier layer capacitors (IBLC) was proposed, and the clarification was acknowledged. It is believed that CCTO is formed of insulating grain boundaries separating semiconducting grains. The IBLC model explains the characteristics of Maxwell–Wagner relaxation in CCTO ceramics [2]

Many scientists have worked to swap trivalent or divalent ions to enhance the CCTO ceramic's dielectric properties. With the substitution of Co^{2+} at the Cu^{2+} site, Kafi et al. tracked down an ascent in dielectric constant [3]. The substitution of Pr^{3+} at the Ca^{2+} site has been displayed to

*Corresponding author, E-mail: srivastava_phy@yahoo.co.in

decrease the dielectric constant and to reduce the dielectric loss [4]. BTO-CCTO composites show a promising capacitor applications for microelectronics and microdevices investigated by Almeida et al. [5] Kushwaha et al. have shown that CCTO can convert solar energy through photochemical and photocatalytic processes. This ability of CCTO makes it a processing material for solar energy conversion technologies [6]. The dielectric properties of CCTO were significantly enhanced by the co-substitution of rare earth and transition metals (Y + Zr), as reported by Xu et al. [7]. According to Li et al. research, the dielectric properties of CCTO showed that adding Sr dopant up to a weight percentage of 0.15 improved both dielectric permittivity and reduced dielectric loss. However, it also reduced frequency dependence at low frequencies [8]. Researchers have been zeroing in decreasing dielectric loss and supporting a high dielectric constant in CCTO by doping or adjusting the preparation method. Grain growth can also be accelerated or slowed by doping [9].

In this research, the physical characteristics of Co–Ni-substituted calcium copper titanate have been investigated. We have used sol–gel auto-combustion method to synthesize $Ca_{1-x}Co_xCu_3Ti_{4-y}Ni_yO_{12}$ ($x = 0.0$, $y = 0.0$; $x = 0.1$, $y = 0.3$; $x = 0.2$, $y = 0.4$).

2. Synthesis of CCTO

$Ca_{1-x}Co_xCu_3Ti_{4-y}Ni_yO_{12}$ ($x = 0.0$, $y = 0.0$; $x = 0.1$, $y = 0.3$; $x = 0.2$, $y = 0.4$) was synthesized through a sol–gel auto-combustion approach. Analytical reagent grade chemicals such as calcium nitrate $(Ca(NO_3)_2)$, cobalt nitrate $(Co(NO_3)_2)$, copper nitrate $(Cu(NO_3)_2)$, titanium dioxide (TiO_2), nickel nitrate $(Ni(NO_3)_2)$, and citric acid $(C_6H_8O_7)$ have been used to synthesize Co–Ni-substituted calcium copper titanate [10, 11]. Stoichiometric proportions of nitrate chemicals have been diluted in 100 ml of distilled water. Citric acid was added in a 1:1 molar ratio to the aqueous solution containing cations. The solution was then put on a magnetic stirrer for 2–3 h at 90–100 °C to get a blue gel when heated at 300 °C on a hot plate, transformed into black fluffy material. The prepared material was then pre-sintered for 6 h at 800 °C to remove impurities. The precursor was further sintered at 900 °C for 6 h before being crushed into a fine CCTO powder using a mortar and pestle.

3. Characterization techniques

The structural properties of the prepared sample were investigated using a Bruker AXS D8 advanced diffractometer to obtain an X-ray diffraction pattern. The pattern was obtained using Cu- Kα radiation at 40 kV and 35 mA within 20–80° with a step size of 0.02°. FTIR spectrophotometer (Nicolet FTIR interferometer prestige-21 model – 8400S) was used to investigate the attached functional groups of the synthesized CCTO in the range of 400–4000 cm^{-1}. FESEM (FEI Nova NanoSEM 450 FESEM) was used to examine the morphology of the synthesized CCTO. The dielectric characteristics were investigated using an impedance analyzer (Wayne Kerr 6500B) with a DC bias voltage of 0 to + 40 V and a DC bias current from 0 to 100 mA in the frequency range of 20 Hz to 1 MHz. The synthesized samples were compressed into disk-shaped pellets using a KBr press with a 6.65 weight percentage of polyvinyl alcohol (PVA) to evaluate the dielectric and impedance analysis.

4. Results and discussions

4.1. XRD analysis

Figure 1(a) shows the XRD pattern of $Ca_{1-x}Co_xCu_3Ti_{4-y}Ni_yO_{12}$ ($x = 0.0$, $y = 0.0$; $x = 0.1$, $y = 0.3$; $x = 0.2$, $y = 0.4$). The existence of the major diffraction (hkl) peaks at (221), (220), (013), (222), (321), (400), (422), and (440) (JCPDS card No. 75–2188) confirms the synthesis of the crystalline structure of calcium copper titanate (CCTO) with space group Im-3. A high-intensity peak having an hkl value (220) has been used to determine the lattice constants. A small amount of secondary phase, such as copper oxide (CuO) (Fig. 1 (a)), with JCPDS card No. 050661 was also present [12]. This may be due to the minor grinding efficiency [13]. The following formulas are used to determine the lattice parameter (a), crystalline dimension (D), and unit cell volume (Vcell).

$$a = d\sqrt{h^2 + k^2 + l^2} \tag{1}$$

$$D = \frac{0.89\lambda}{\beta\cos\theta} \tag{2}$$

$$V_{cell} = a^3 \tag{3}$$

where θ is Bragg's angle and β is FWHM in radians. It can be seen from Table 1 that the lattice parameters and volume of the unit cell are slightly decreasing with an increasing concentration of substituted Co–Ni. This might be due to the difference in ionic radii of Co^{3+} (0.60 Å), Ca^{2+}(0.990 Å), Ti^{4+} (0.605 Å), and Ni^{2+} (0.690 Å) [14]. The observed increase in lattice parameters resulting from the substitution of Ni 2 + for Ti4 + is believed to be due to the larger ionic radius of Ni^{2+} (0.690 Å) compared to the host Ti^{4+} (0.605 Å). This increase is thought to counteract the negative effect of substituting Co^{3+} (0.60 Å) for
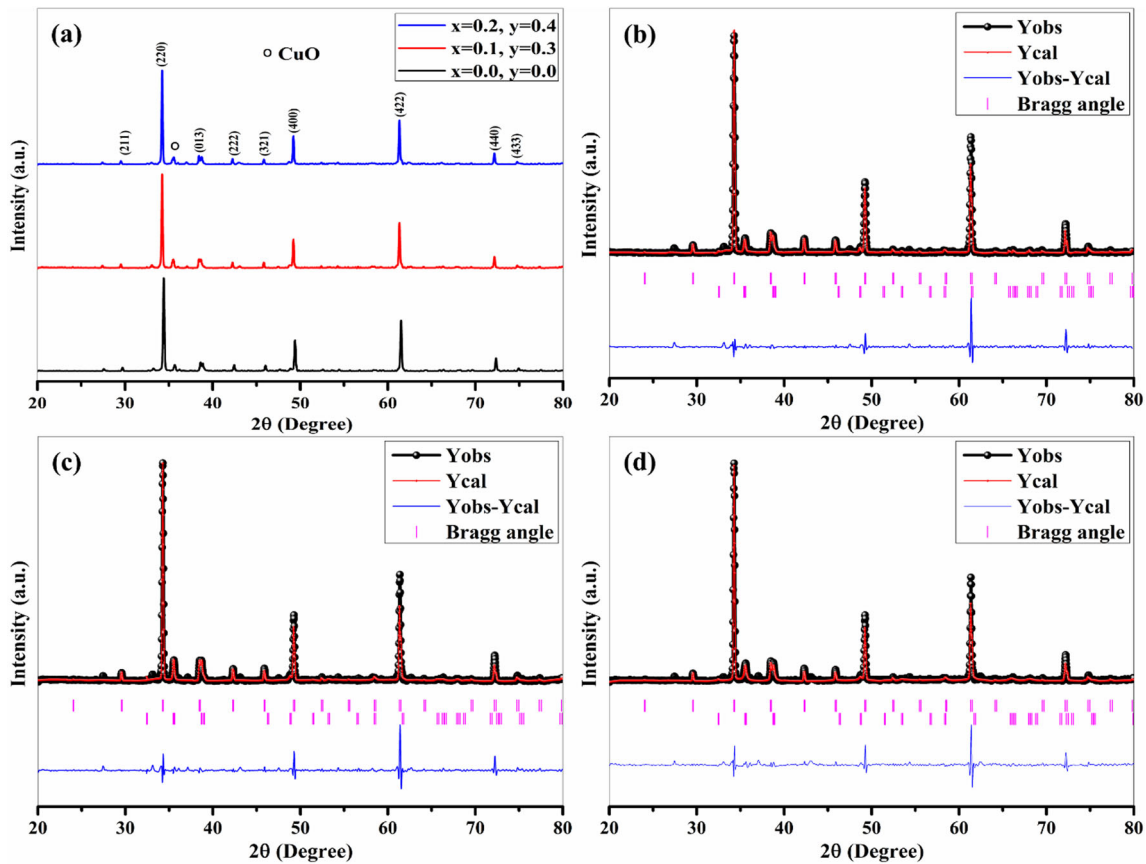
Fig. 1 (**a**) XRD pattern of $Ca_{1-x}Co_xCu_3Ti_{4-y}Ni_yO_{12}$ ($x = 0.0$, $y = 0.0$; $x = 0.1$, $y = 0.3$; $x = 0.2$, $y = 0.4$), Rietveld refinement (**b**) $x = 0.0$, $y = 0.0$; (**c**) $x = 0.1$, $y = 0.3$; (**d**) $x = 0.2$, $y = 0.4$

Ca^{2+}(0.990 Å). This expansion is consistent with the findings of other researchers in the field [15–17]. The refinement of XRD patterns was done using FullProf suite software. The pseudo-Voigt function was used to improve the peak morphology, and linear interpolation was used to represent the background. The black line shows the experimental data, the blue line shows the difference between the calculated fitted data and the experimental data, and the red line shows the calculated fitted data [18]. The lines in pink color represent the Bragg angle of each peak for both the CCTO and CuO phases. The considered conditions to realize this refinement are given in Table 1. From refined XRD patterns (Figs. 1 (b), (c) and (d)), we can observe that the experimental plot (Yobs) properly matches the theoretical plot (Ycal) since the CuO phase was also refined. The reliability factors (R_p, R_{wp}, and R_{exp}), the goodness of fit (GoF), and chi-square (χ^2) are displayed. Other factors that support the fit's validation include $28.2\% \leq R_p \leq 34.5\%$, $30.4\% \leq R_{wp} \leq 37.4\%$, $32.9\% \leq R_{exp} \leq 34.9\%$, and $0.91 \leq \text{GoF} \leq 1.1$.

4.2. FTIR analysis

FTIR spectra of $Ca_{1-x}Co_xCu_3Ti_{4-y}Ni_yO_{12}$ ($x = 0.0$, $y = 0.0$; $x = 0.1$, $y = 0.3$; $x = 0.2$, $y = 0.4$) in the range of 400 to 4000 cm^{-1} are shown in Fig. 2. The major bands are found to correspond to 422 cm^{-1}, 503 cm^{-1}, and 556 cm^{-1}. The metal–oxygen bonds stretching vibration mode might generate these bands [19]. Because of the accumulated vibrations of CuO_4 and TiO_6 octahedrons, absorption bands occur between 380 and 700 cm^{-1}, confirming the presence of CCTO structure as shown in XRD. The intensity of the peaks 422 cm^{-1}, 503 cm^{-1}, and 556 cm^{-1} tends to decrease with the increase in Co–Ni substitution [20, 21]. A peak at 2366 cm^{-1} is due to the presence of Co_2 in the prepared samples [22]. The band observed at 1519 cm^{-1} and at around 3743 cm^{-1} might be ascribed due to the C-H vibrations of alkyl groups and the O–H vibrations of water molecules found in the prepared material [23, 24].

4.3. FESEM analysis

Figure 3 shows the FESEM micrographs and grain size distribution of CCTO. From Fig. 3a, c, and e, the prepared

Table 1 Lattice constants (a), d spacing (d), diffraction angle (2θ), full width at half maxima (β) and volume of the unit cell (V) for $Ca_{1-x}Co_xCu_3Ti_{4-y}Ni_yO_{12}$ (x = 0.0, y = 0.0; x = 0.1, y = 0.3; x = 0.2, y = 0.4)

Sample code	x = 0.0, y = 0.0	x = 0.1, y = 0.3	x = 0.2, y = 0.4
λ (Å)	1.54056	1.54056	1.54056
Cycles of refinement	30	30	30
Step (°)	0.020	0.020	0.020
Profile function	P-Voigt * Axial divergence asymmetry	P-Voigt * Axial divergence asymmetry	P-Voigt * Axial divergence asymmetry
R_p (%)	28.2	32.0	34.5
R_{wp} (%)	30.4	32.8	37.4
R_{exp} (%)	32.9	34.0	34.9
β (°)	0.127	0.079	0.074
D (nm)	64.79	104.10	111.13
(2θ)	34.42	34.23	38.46
d (Å)	2.6036	2.6172	2.3386
A (Å)	7.36	7.40	7.39
V (Å³)	399.35	405.64	405.12
a (Å) (Rietveld)	7.401139	7.398353	7.399135
V_{cell} (Å³) (Rietveld)	405.411 (0.015)	404.954 (0.017)	405.082 (0.018)
χ^2	0.8506	0.9318	1.147
GoF	0.91	0.95	1.1
Bragg R-factor (%)	7.26	9.16	14.5
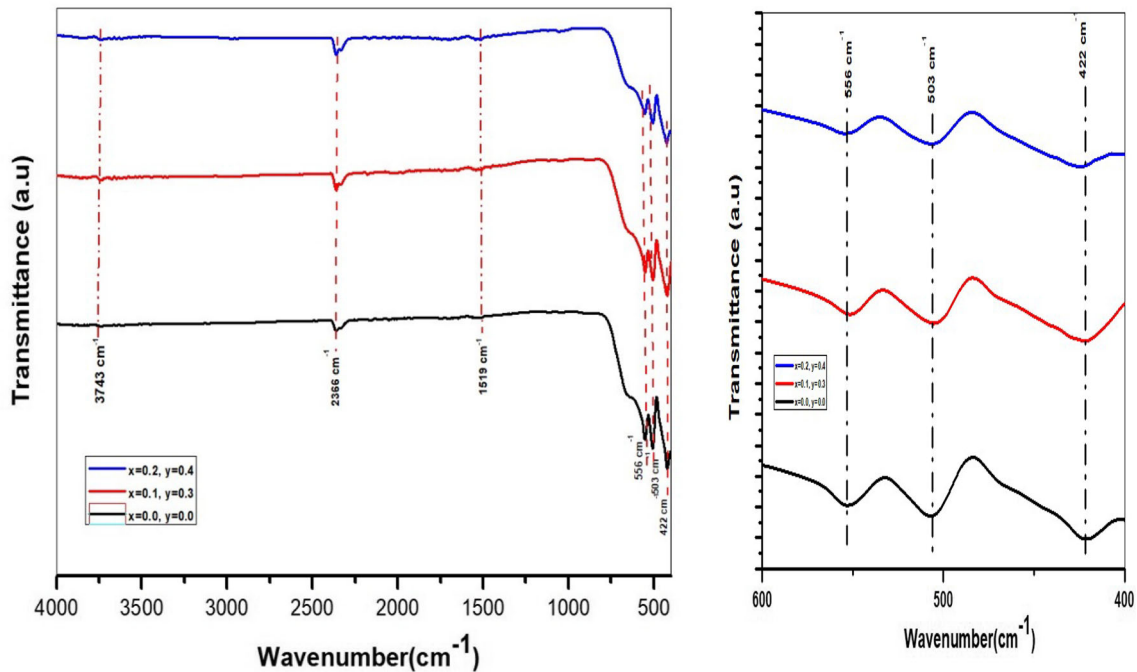
Fig. 2 FTIR spectra of $Ca_{1-x}Co_xCu_3Ti_{4-y}Ni_yO_{12}$ (x = 0.0, y = 0.0; x = 0.1, y = 0.3; x = 0.2, y = 0.4)

sample shows a homogeneous distribution of particles with non-uniformity shapes. Figure 3b, d, and f depicts the distribution of the particle size, and it was noticed that it follows the normal law distribution. From these figures, we evaluated the average grain sizes, which were found to be 0.35 μm for (x = 0.0, y = 0.0), 0.58 μm for (x = 0.1, y = 0.3), and 0.72 μm for (x = 0.2, y = 0.4). It was observed that the grain size increases with an increase in the concentration of Co–Ni substitution. The reason behind this increase can be related to the fact that the host atoms
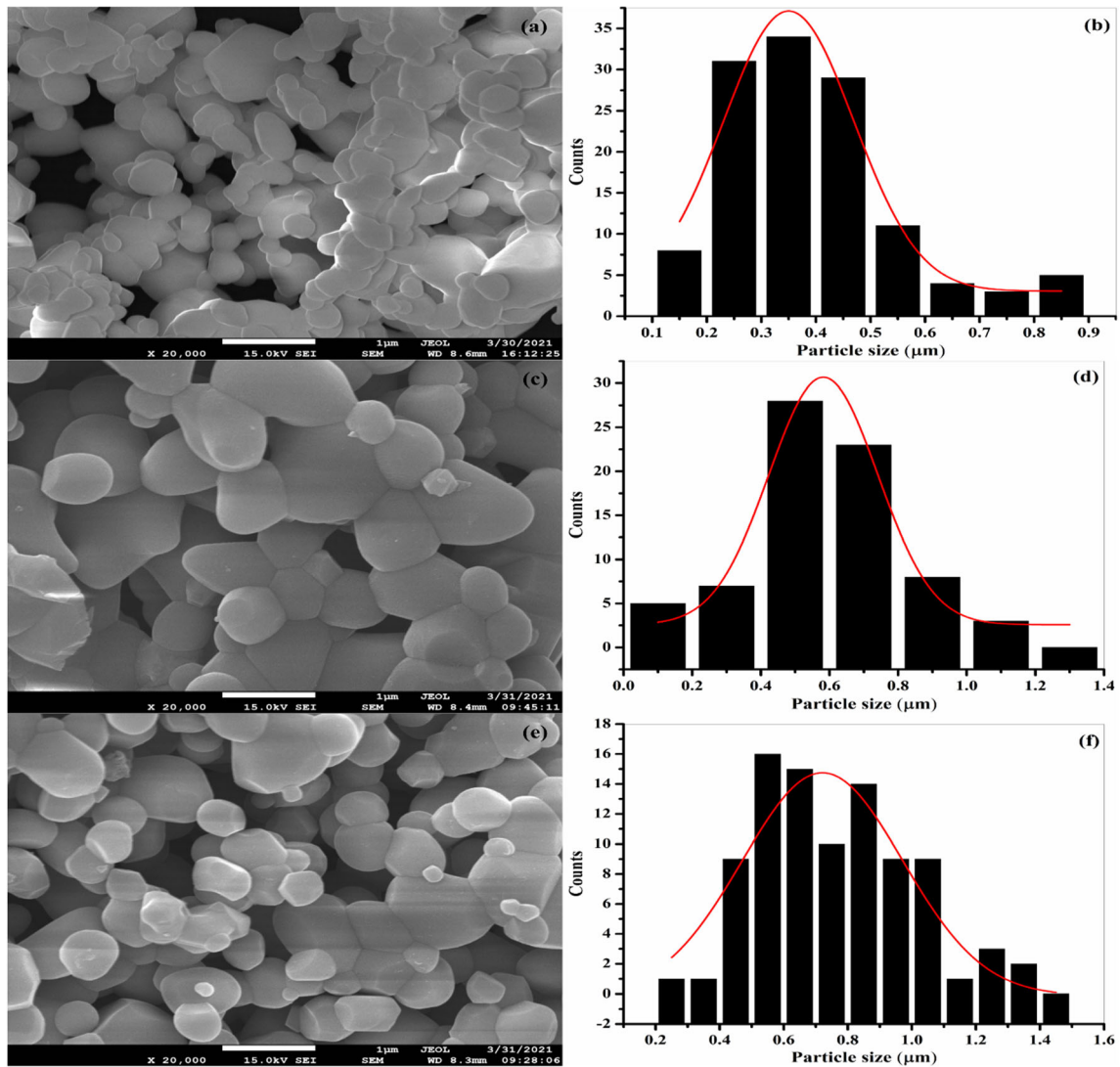
Fig. 3 FESEM micrographs of $Ca_{1-x}Co_xCu_3Ti_{4-y}Ni_yO_{12}$ (**a**) $x = 0.0$, $y = 0.0$; (**c**) $x = 0.1$, $y = 0.3$; (**e**) $x = 0.2$, $y = 0.4$ and particles size distribution of $Ca_{1-x}Co_xCu_3Ti_{4-y}Ni_yO_{12}$ (**b**) $x = 0.0$, $y = 0.0$; (**d**) $x = 0.1$, $y = 0.3$; (**f**) $x = 0.2$, $y = 0.4$

(Ca and Ti) are paramagnetic, while the substituted atoms (Co and Ni) are ferromagnetic. Increasing the magnetic moment in the samples would favor the magnetic interaction during the synthesis, which could affect the particle size obtained.

4.4. Dielectric analysis

4.4.1. Dielectric constant

The ability to understand a material's electric behavior requires dielectric characterization. The dielectric response is influenced by preparation techniques, heating temperature, duration, sample concentration, and cation substitution. These parameters determine the sort of conduction and polarization processes used, such as ionic, interfacial polarization, dipolar, and electronic. The following equation calculates the complex permittivity (ε^*) of the prepared sample [25].

$$\varepsilon^* = \varepsilon' - j\varepsilon'' \tag{4}$$

where j $= \sqrt{-1}$, complex integer, ε' is the real component of complex permittivity, and ε'' is the imaginary component of complex permittivity.

$$\varepsilon' = \frac{z''}{\omega c_0 z^2} \tag{5}$$

$$\varepsilon'' = \frac{z'}{w C_0 z^2} \tag{6}$$

Z' denotes the real part of complex impedance, while Z" denotes the imaginary part of complex impedance. $\omega = 2\pi f$, where C stands for capacitance.

Figure 4 (a) illustrates the fluctuation of the dielectric constant against frequency for CCTO at room temperature throughout a frequency range of 100 Hz to 1 MHz. Dielectric materials exhibit a response to an applied electric field, which is described by the net polarization of the material. The polarization arises from various mechanisms, including space charge polarization, dipole polarization, ionic polarization, and electronic polarization. Together, these polarization mechanisms contribute to the overall response of the dielectric material to an external electric field [26]. At lower frequencies, space charge polarization is dominant, while at higher frequencies, electronic polarization becomes more significant. In the intermediate frequency range, dipole and ionic polarization play a more prominent role in determining the dielectric response. Figure 4(a) shows that the prepared samples show larger value of ε' at lower frequencies. Value of ε' is 3224 for $x = 0.0/y = 0.0$, 2263 for $x = 0.1/y = 0.3$, and 2957 for $x = 0.2/y = 0.4$ at 100 Hz. The high dielectric constant observed at lower frequencies indicates the presence of charge carriers that accumulate at the interface between the grains and grain boundaries, leading to the space charge polarization [27]. This explanation is based on the Maxwell–Wagner model, which states that dielectric materials with a heterogeneous structure can be considered consisting of conducting grains and insulating grain boundaries. This configuration results in the development of polarization due to the accumulation of space charge at the grain boundaries when an electric field is applied [27, 28].

As observed in the CCTO electro-ceramic with $x = 0.1/y = 0.3$, low concertation of Co–Ni decreases the value of ε'. As the concentration of Co–Ni increases having $x = 0.2/y = 0.4$, the value of ε' increases. The value of ε' across all the samples exhibits a gradual decrease as the frequency increases until higher frequencies where a significant rise in ε' is observed in samples. This sudden increase in ε' at higher frequencies can be attributed to electronic polarization [29]. From Fig. 4(b), values of ε'' are 1838 for $x = 0.0/y = 0.0$, 681 for $x = 0.1/y = 0.3$, and 1123 for $x = 0.2/y = 0.4$ at 100 Hz. As shown from the figure, ε'' shows a similar behavior as ε' in prepared samples with the dopant concentration of Ni and Co. It is noticed that as the frequency increases, the imaginary part of the dielectric decreases and eventually reaches a stable value, becoming independent of frequency in the high-frequency range. This behavior can also be explained based on Maxwell–Wenger model. This model explains that in low-frequency range, the grain boundaries are more influential, while the grains play a larger role in the high-frequency range. At low frequency, electrons tend to accumulate in the grain boundaries, which have high resistivity, making electron hopping requires more energy and resulting in a higher loss. Conversely, at high frequencies, the highly conductive grains become more active, enabling electron exchange to occur with less energy, thereby reducing the dielectric loss [30]. This similar behavior is also observed by T. Hussain et al. [31]

4.4.2. Dielectric loss

The energy of dissipation in a dielectric system is represented by the dielectric tangent loss factor. Dielectric loss can be calculated by using the following equation:

$$\tan \delta = \frac{\varepsilon''}{\varepsilon'} \tag{7}$$

Figure 5 illustrates that for the samples $Ca_{1-x}Co_xCu_3Ti_{4-y}Ni_yO_{12}$ ($x = 0.0$, $y = 0.0$; $x = 0.1$, $y = 0.3$; $x = 0.2$,
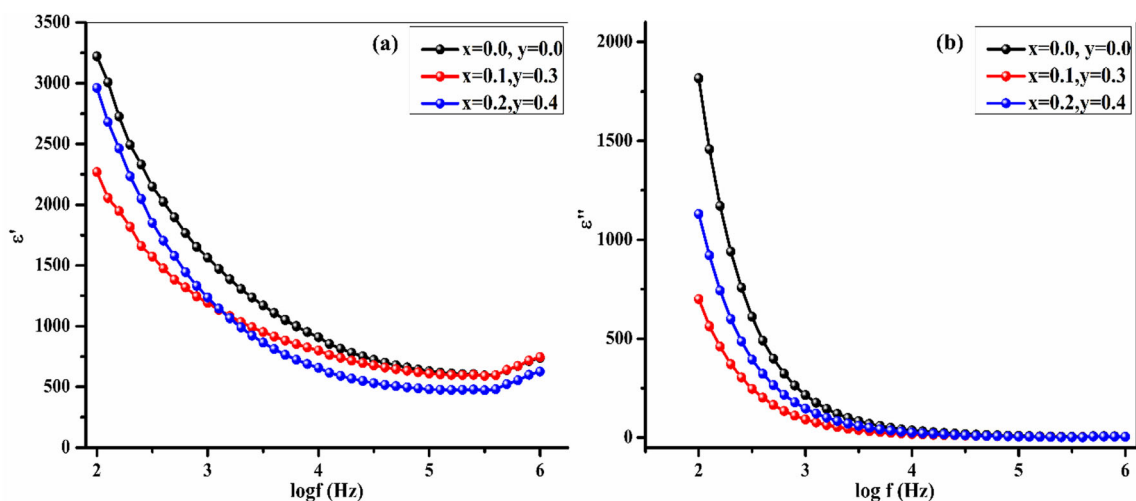
Fig. 4 (a) Variation of dielectric constant (ε') versus frequency and (b) imaginary part of dielectric (ε'') versus frequency for $Ca_{1-x}Co_xCu_3Ti_{4-y}Ni_yO_{12}$ ($x = 0.0$, $y = 0.0$; $x = 0.1$, $y = 0.3$; $x = 0.2$, $y = 0.4$)

$y = 0.4$), the dielectric losses are 0.96, 0.52, and 0.65 at 100 Hz. It is evident that the tan δ of all CCTO ceramics exhibits a gradual decrease in the range of 100 Hz to 10^5 Hz, followed by a sharp increase in the high-frequency range of 10^5 Hz to $10.^7$ Hz. This sharp rise in dielectric loss may be due to the resonance effect arising from the stray conductance of contacts and leads [10, 32]. When the concentration of doped Co–Ni increases, tan δ decreases. This behavior can also be discussed based on structural imperfections that produce electrical polarization, and dielectric loss gradually rises at higher frequencies. Similar behavior is observed by Liu et al. [33]

4.4.3. Impedance analysis

Polycrystalline materials with heterogeneous nature exhibits several electrical characteristics due to grain and grain boundary [34]. The grain resistance (R_g) and grain boundary resistance (R_{gb}) responses to the dielectric response may be determined using the phenomenon of the semicircular arc shown in the plot Z" versus Z', often known as the Nyquist plot. Z* is a complex impedance that may be written as

$$z^* = z' - iz'' \qquad (8)$$

The semicircles were obtained for all the samples (Fig. 6). These graphs represent that grain boundary density is the most critical factor in conduction. Grain resistance determines the left half of the semicircle, i.e., the lower frequency side. On the other hand, the grain boundary influences on the intermediate frequencies [35, 36]. The total resistance of both grain and grain boundaries is defined by the extreme right side in the high-frequency zone [37]. Because of the addition of concentration of Co–Ni substitution, the grain resistance starts increasing and then subsequently drops due to the increase in the concentration of Co–Ni substitution. A similar pattern is observed by Yang et al. [38] indicating that the grain resistance is smaller than the grain boundary resistance. The sample $x = 0.2/y = 0.4$ shows the presence of a secondary phase, CuO, which results in low dielectric loss with high grain boundary resistance. This same behavior was observed by Li et al. [39]. To establish a correlation between microstructure and electrical properties, experimental data are often modeled using an ideal equivalent circuit that incorporates resistance and capacitance. Many other researchers also used the equivalent circuit to extract the parameters (R_g, R_{gb}, C_g) that play a role in determining the electrical conductivity and resistivity of prepared samples [40, 41]. The fitting of this data was performed using EIS ANALYSER software, and the resulting fit data is presented in Table 2. The equivalent circuit used for a good fitting is shown in Fig. 6 (inset). The samples analyzed in our study show a greater contribution from grain boundary resistance (R_{gb}), as evidenced by the absence of a semicircular arc in the high-frequency region. Based on these observations, the majority of the dielectric properties of the prepared samples arise from R_{gb}. It can be inferred that in the case of CCTO ceramics, the contribution of R_g to the dielectric properties is negligible as compared to R_{gb} [42]. Our sample exhibits higher resistance in the low-frequency region; it is reasonable to assume that an intrinsic grain boundary relaxation process is dominant, which is primarily governed by the grain boundary. This can be attributed to the insulating nature of the grain boundary,
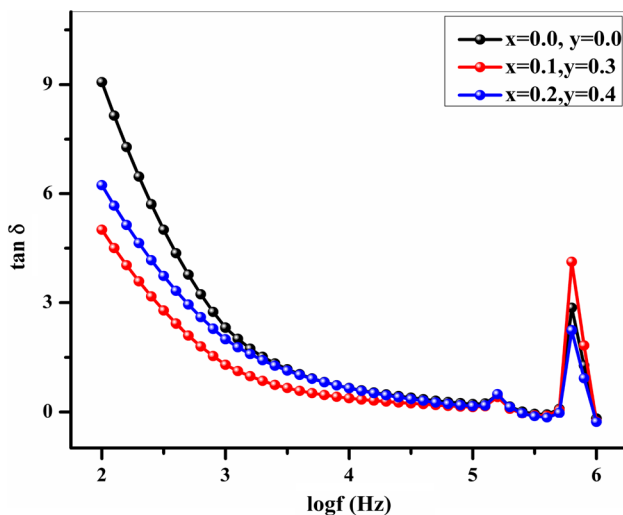

Fig. 5 Variation of dielectric loss tangent with frequency for $Ca_{1-x}Co_xCu_3Ti_{4-y}Ni_yO_{12}$ ($x = 0.0$ $y = 0.0$, $x = 0.1$ $y = 0.3$, $x = 0.2$ $y = 0.4$)
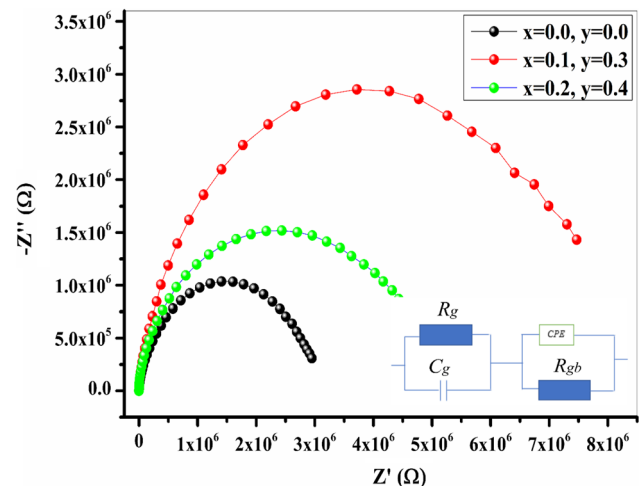
Fig. 6 Nyquist plot of complex impedance for $Ca_{1-x}Co_xCu_3Ti_{4-y}Ni_yO_{12}$ ($x = 0.0$ $y = 0.0$, $x = 0.1$ $y = 0.3$, $x = 0.2$ $y = 0.4$)

Table 2 R_g, C_g, and R_{gb} of the compound $Ca_{1-x}Co_xCu_3Ti_{4-y}Ni_yO_{12}$

Concentrations	R_g (Ω)	C_g (F)	R_{gb} (Ω)
$x = 0.0$, $y = 0.0$	8.7769E-8	5.8795E-10	3.0372E6
$x = 0.1$, $y = 0.3$	9.0546E-8	2.6716E-19	8.063E6
$x = 0.2$, $y = 0.4$	1.0074E-8	9.9514E-20	4.997E6

which prevents the charge carriers from moving freely and confines them near the grain boundary [43].

5. Conclusions

Using the sol–gel technique, we have synthesized and analyzed Co–Ni substituted calcium copper titanate. The secondary phase, such as CuO, has been observed in the XRD patterns of the prepared samples. The microstructure shows large grain sizes ranging from 0.35 μm to 0.72 μm. A steady increase in dielectric loss at higher frequencies has been observed, which might be owed to structural defects that can also cause electronic polarization. The grain boundary resistance has a major contribution to the dielectric properties of synthesized calcium copper titanate, as seen by the Cole–Cole plot. This dominant contribution of R_{gb} to the dielectric properties allows for the design of high-capacitance capacitors with minimal energy loss due to dielectric heating and signal attenuation, making it a promising material for use in advanced electronic technologies.

Declarations

References

[1] P Thomas *J. Eur. Ceram. Soc.* **32** 1681 (2011)

[2] J Wang, J Wang, R Xu, Y Sun, B Zhang and W Chen *J. Alloys Compd.* **653** 14 (2015)

[3] Z Kafi and A Kompany *J. Alloys Compd.* **727** 168 (2017)

[4] A K Rai, N K Singh, S K Lee and K D Mandal *J. Alloys Compd.* **509** 8901 (2011)

[5] A F L Almeida, P B A Fechine, L C Kretly and S B Sombra *J. Mater. Sci.* **41** 4623 (2006)

[6] H S Kushwaha, N A Madhar, B Ilahi, P Thomas, A Halder and R Vaish *Sci. Rep.* **6** 10 (2016)

[7] Z Xu, H Qiang and Y Chen *Chen Mater. Chem. Phys.* **191** 1 (2017)

[8] T Li, D Liu, H Dai, H Xiang, Z Chen, H He and Z Chen *J. Alloys Compd.* **599** 145 (2014)

[9] S H Hong, D Y Kim and H M Park *J. Am. Ceram. Soc.* **90** 2118 (2007)

[10] K D Mandal and A K Rai *J. Alloys Compd.* **478** 771 (2009)

[11] A K Rai and K D Mandal *J. Alloys Compd.* **491** 507 (2010)

[12] S N Kane, A Mishra and A K Dutta *J. Phys. Conf. Ser.* **755** 1 (2016)

[13] D Capsoni, M Bini, V Massarotti, G Chiodelli, M C Mozzatic and C B Azzoni *J. Solid State Chem.* **177** 4494 (2004)

[14] Z Zhang, X Liu, X Wang and Y Wu *J. Alloys Compd.* **525** 114 (2012)

[15] I Ali, M U Islam, M Naeem, H M Khan and M A Iqbal *Mater. Res. Bull.* **49** 338 (2013)

[16] M J Iqbal and S Farooq *Mater. Res. Bull.* **44** 2050 (2009)

[17] S Ounnunkad *Solid State Commun.* **138** 472 (2006)

[18] G Mukhtar, J Mohammed, T T T Carol, N Halilu, S Sharma, U M Isah, S K Godara and A K Srivastava *Solid State Sci.* **113** 106549 (2021)

[19] A H Najafabadi *Ceram. Int.* **42** 13625 (2016)

[20] T Xie, L Xu and C Liu *Powder Technol.* **232** 87 (2012)

[21] T A Alrebdi et al. *Mater. Sci. Eng. B Solid-State Mater. Adv. Technol.* **280** 115682 (2022)

[22] J Mohammed, T T T Carol, H Y Hafeez, D Basandrai, G R Bhadu, S K Godara, S B Narang and A K Srivastava *Res. Phys.* **13** 102307 (2019)

[23] M Feng and X Huang *Eng. Asp.* **441** 556 (2014)

[24] A S Attar, E S Sichani and S Sharafi *J. Mater. Res. Technol.* **6** 108 (2017)

[25] J Mohammed, T T T Carol, H Y Hafeez, B I Adamu, Y S Wudil, Z I Takai, S K Godara and A K Srivastava *J. Phys. Chem. Solids* **126** 85 (2019)

[26] L Singh, U S Rai, K D Mandal and N B Singh *Prog. Cryst. Growth Charact. Mater.* **60** 15 (2014)

[27] S Jesurani and S Kanagesan *J. Mater. Sci. Mater. Electron.* **23** 668 (2012)

[28] M J Iqbal, M N Ashiq and I H Gul *J. Magn. Magn. Mater.* **322** 1720 (2010)

[29] L Singh, U S Rai, K Mandal, B C Sin, S I Lee and Y Lee *Ceram. Int.* **40** 10073 (2014)

[30] Z Maleknejad, K Gheisari and A H Raouf *J. Supercond. Nov. Magn.* **29** 2523 (2016)

[31] T Hussain, S A Siddiqi, S Atiq and M S Awan *Prog. Nat. Sci. Mater. Int.* **23** 487 (2013)

[32] J Mohammed et al. *Springer International Publishing* **369** (2018)

[33] P Liu, Y Lai, Y Zeng and S Wu *J. Alloys Compd.* **650** 59 (2015)

[34] J Liu, C G Duan and W N Mei *J. Appl. Phys.* **98** 1 (2005)

[35] Y Bai and J Zhou *J. Magn. Magn. Mater.* **278** 208 (2004)

[36] M G Chourashiya and J Y Patil *Chem. Phys.* **109** 39 (2008)

[37] H Malik, M A Khan, A Hussain and M F Warsi *Int.* **44** 605 (2018)

[38] Z Yang, L Zhang and X Chao *J. Alloys Compd.* **509** 8716 (2011)

[39] W Li and S Qiu *J. Mater. Sci. Technol.* **26** 682 (2010)

[40] L. Sahoo, S. Bhuyan, and S. N. Das *Appl. Phys. A Mater. Sci. Process.* **128** 1 (2022)

[41] S N Das, S Pradhan, S Bhuyan and R N P Choudhary *Das J. Electron. Mater.* **46** 1637 (2017)

[42] J Li, R Jia, L Hou, L Gao and K Wu *Li J. Alloys Compd.* **644** 824 (2015)

[43] J Mohammed et al. *Ceram. Int.* **46** 7187 (2020)